The Zeeman effect: An experiment to determine the splitting of energy levels in an external magnetic field.

Jacob Gordon (201416406)

Department of Physics, The University of Liverpool.

19th of October 2021

Abstract:

Using a Cadmium lamp surrounded by an electromagnet, the splitting of energy levels was accurately measured This was then used to determine several values for the Bohr magnetron and find the polarisation states. One of these values was $1.022e-23 \pm 2.056e-24\ J/T$, overall, the experiment was successful.

1. Introduction

The normal Zeeman effect is the splitting of energy levels in an external magnetic field, in which the magnetic field strength is proportional to the splitting. The Zeeman effect was discovered by Dutch physicist Pieter Zeeman in 1896 [1] when he burned Hydrogen [2] to produce a spectrum and subjected it to an external magnetic field. He noticed that the spectral lines began to double or even triple in some cases.

At this point in time the electron had not been discovered so Zeeman was quite perplexed by what he had found. Today it is known that the Zeeman effect is the outcome of electron spin in a magnetic field. When splitting occurs electrons of opposite spin transition to different energy levels [1]. Zeeman's findings were announced by Oliver Lodge in 1897 at the Royal Society of London and he was later awarded the Nobel Prize in 1902. The Zeeman effect is used currently to help better identify angular momenta in atoms by determining their energy levels. It also provides an effective means of studying atomic nuclei [3].

The main purpose of this experiment was to find a value for the Bohr magneton and to determine the polarisation states for the Zeeman transitions and compare them to the known values. This was done by measuring the splitting of the energy levels when under the influence of a magnetic field for both transverse and longitudinal waves. For the polarisation states the same thing was done except polarisation filters were used to observe the splitting. A cadmium (Cd) light source was used for this experiment. A Fabry-Perot etalon was used to examine the splitting of the red Cd spectral lines being at a wavelength of 643.847nm. More details of how the experiment was conducted can be found in the methodology.

2. Theory

In the normal Zeeman effect, the magnetic field interacts with the orbital angular momentum of the atomic energy levels. The equation that governs the total angular momentum **is J = L + S** (Where L is orbital angular momentum and S is the spin angular momentum). However, in this experiment the transitions were between the energy levels $^1D_2$ and $^1P_1$ which both have a spin angular momentum of S = 0. This means that only L the orbital momentum contributed to the total momentum J (**J = L)**, this means that the magnetic moment can be written as:

$$\mu = -\frac{e}{2m_e}L = \frac{\mu_B}{h}J$$

Equation 1 – the magnetic moment.

The definition for all the variables in this equation and in equations further on in this report can be found in appendix B. Following on from equation 1, the potential energy of a magnetic moment is defined as:

$$E = -\mu B$$

Equation 2 – The potential energy of a magnetic moment in B.

The total angular momentum J and the external magnetic field B are both quantised (by the quantum number M). This means that the electrons in this system are restricted and can only hold certain values [4], hence the electrons can only travel to certain different energy levels depending on which level they are already in. When the magnetic field splits the energy levels will be separated equidistantly by the equation:

$$\delta E = \mu_B B$$

Equation 3 – The potential energy during splitting.

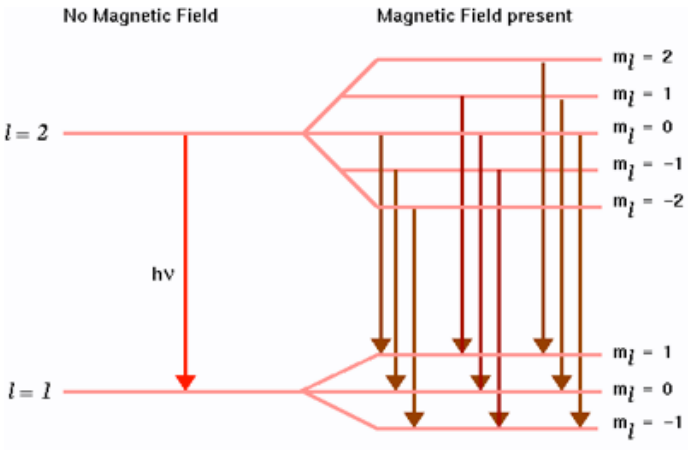

Figure 1 – An image to show the change in energy levels during splitting.

Figure 1 shows the energy level transitions possible between the $^1D_2$ and $^1P_1$ states ($^1D_2$ at the top and $^1P_1$ at the bottom), the transitions are governed by the selection rules $\Delta M = 0, \pm 1$ and $\Delta L = \pm 1$. This can be seen in figure 1, for example the electron in the M = 2 level for the $^1D_2$ state can only transition to M = 1 for the $^1P_1$ state. Whereas the election in the M = 0 level can transition to any other energy level.

Given the fact we have the wavelength, we can calculate the energy separation between the states for B = 0 and for B = 500mT.

$$E_0 = \frac{hc}{\lambda_0}$$

Equation 4 – The initial energy of the system.

Using equation 4 and the initial wavelength of 643.847nm an initial energy 1.93077ev was found when no magnetic field was applied. To calculate the energy separation when the magnetic field was in place was not as simple.

$$\mu_B = \frac{eh}{2m_e}$$

Equation 5 – Bohr magneton

Equation 5 was then combined with equation 3 to find a value for δE.

$$\delta E = \frac{eh}{2m_e}B$$

Equation 6 – A different equation for the potential energy during splitting.

After calculating δE using equation 6 where B was 500mT, we found the value of δE to be 2.8957e-5. To get the final two energy separations this value must be taken away and added to our initial value E_0. Doing this we get $E_0 + \delta E = 1.930799ev$ and $E_0 - \delta E = 1.930748ev$. The three values for energy separation are all very similar. These values also show that three distinct energy transitions are possible.

Two different types of Zeeman effect can be observed. The first is the "normal" Zeeman effect, which has already been discussed and happens when there is no spin magnetic moment, leading to even splitting. The other type of Zeeman effect is the "anomalous" Zeeman effect, and this is where the effects of

splitting can be more complex. As there may be spin on some of the electrons causing uneven splitting, or in some cases the magnetic field splits four or more lines, showing wider spacing than anticipated [2].

To observe the change in the energy levels, the shifts in the wavelength are resolved using a spectrometer called a Fabry-Perot etalon.

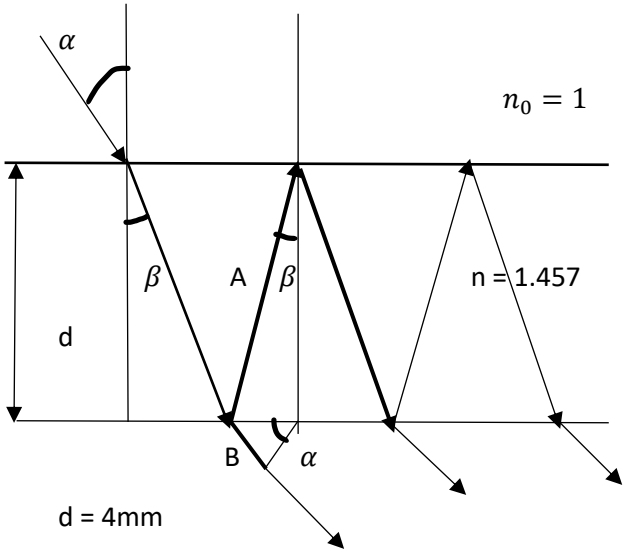

Figure 2 – The light path through a Fabry-Perot etalon for constructive interference.

Figure 2 shows what a Fabry-Perot etalon does in practise. As a light ray enters at the angle α it is reflected internally a few times, with each reflection. A small amount of light escapes which is what produces the interference patten. To get the constructive interference, the optical path difference (OPD) must be equal to an integer value k of the wavelength.

$$OPD = k\lambda = 2nA - B$$

Equation 7 – The optical path difference.

In this form, equation 7 is not usable, however using trigonometry and Snell's law we can convert it to be in terms of a, d, and n.

$$OPD = k\lambda = 2d\sqrt{n^2 - \sin(a)^2}$$

Equation 8 – The Etalon equation.

This equation can then be rearranged to calculate values for α.

$$\alpha = sin^{-1}(\sqrt{n^2 - \left(\frac{k\lambda}{2d}\right)^2})$$

Equation 9 – The Etalon equation rearranged for α

Using this equation values for the angle α can be calculated. Using α the values for the radii fringes can be calculated.

This process of calculating α, while accurate is not always practical as it is not possible to determine values for d and k. This means that in this experiment we had to derive an expression for α which was independent of k and d.

$$\frac{\Delta\lambda}{\lambda_0} = \frac{\sqrt{n^2 - \sin(\alpha_1)^2}}{\sqrt{n^2 - \sin(\alpha_0)^2}} - 1$$

Equation 10 – The difference in wavelength over the initial wavelength.

Equation 10 is a rearrangement of equation 8 by taking the difference in two wavelengths (full derivation in appendix B).

3. Methodology

This experiment was performed twice, once for Transverse waves and the other for Longitudinal.

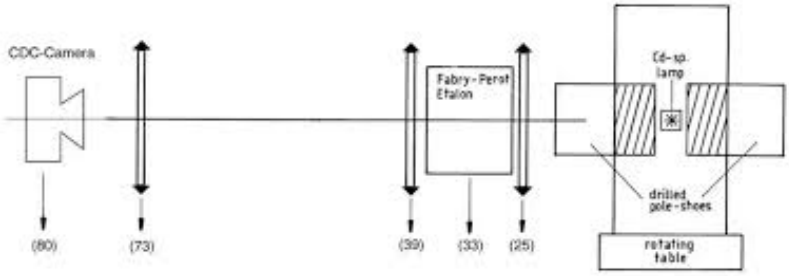

Figure 3 – An illustration of the equipment used to perform the experiment.

Before the experiment could begin, the equipment had to be set up and calibrated. Figure 3 shows a basic version of the equipment used in this experiment; it consists of the charged couple device (CCD) camera which works by using a light sensor in an integrated circuit to convert an electrical signal into an output [5]. In this case the

camera converts the light given off during the constructive interference. The equipment also consisted of a condenser and imaging lens; the condenser lens will align the light produced by the Cd lamp into a straight path [6] allowing the maximum amount of light to reach the CCD camera. The imaging lens sees to magnify the light, both lenses had a focal length of $150mm \pm 1mm$.

The Cd lamp itself is surrounded by an electromagnet; this is how the external magnetic field is applied. To change from Transverse to longitudinal the electromagnet is rotated 90°. Unshown on figure 3 was a red filter. This was used to split the light into the wavelength of 643.847nm as mentioned in the theory. The final piece of equipment used was an eyepiece. This was used to look at the constructive interference patten produced by the Fabry-Perot etalon and was used to calibrate the system.

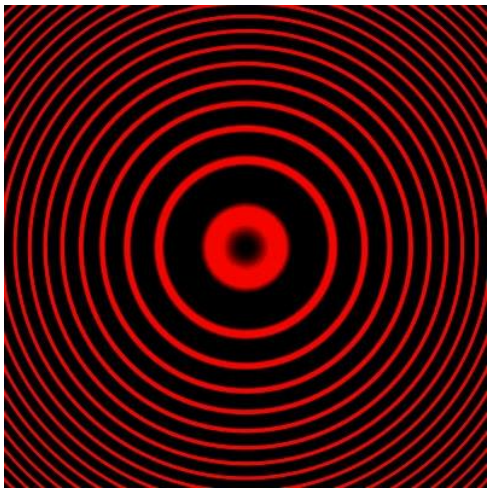

Figure 4 – An example of the constructive interference produced by the Fabry-Perot etalon.

To calibrate the system, the centre ring shown in figure 4 had to line up with the crosshair of the eyepiece. To make sure this happened the position of the lenses were corrected and the 3 adjustable screws on the etalon modified. The condenser and imaging lens were originally set at 13.5cm and 79cm away from the Cd lamp, respectively. When looked through the eyepiece the image appeared blurry, to correct this the lenses were then moved back and forth until a sharp image was produced. At this point the image still was not calibrated as the crosshair on the eyepiece did not match up with the centre ring. The three screws on the Etalon were then moved until the crosshair lined up. Once the system was calibrated the eyepiece was then swapped out for the CCD camera.

To produce a magnetic field current had to be applied to the electromagnet. It was initially decided that measurements would be taken at 0A and move up to 8.0A in 0.5A steps. However, this was later changed to take measurements from 5.0A to 8.0A in steps of 0.2A. This is because no splitting can be seen until at least 5.0A, as the magnetic field was not strong enough. it was decided it would be more practical to get more readings at a higher current. The relationship between the current and magnetic field is as follows:

$$B = -0.9421I^3 + 6.1937I^2 + 86.975I + 7.3701$$

Equation 11 – The relationship between current and magnetic field.

Readings were recorded using software called videoCom intensities. The CCD camera was plugged directly into a PC so the output could be viewed in real time. Once the data had been recorded and saved the next measurement was taken. The process was conducted for transvers waves and then repeated for longitudinal waves. This means thirty separate graphs were plotted in total (see results and analyses examples of these graphs).

After all data was collected, data was then collected to establish the polarisation states. The current for this part of the experiment had to remain consistent otherwise more than one variable would be being changed. 6.0A was chosen because a high current is needed to accurately see the splitting of the energy levels. Like the rest of the experiment both transverse and longitudinal waves would be examined.

The polarisation filter was on a scale from 0° to 90°, data was taken in intervals of 10° to

get an accurate representation of how the splitting changed with the angle. Once this process was complete for both waves it was then repeated with the quarter-wave plate.

4. Results and Analysis

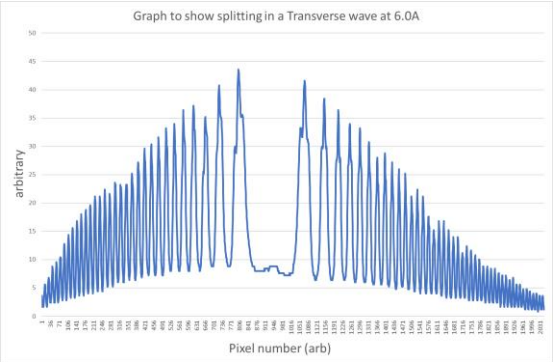

Figure 5 – A graph to show splitting in a transverse wave at 6.0A

Observed in figure 5, the two central peaks show splitting of the energy levels. It was stated in the methods that data was taken from 5.0A onwards. However only graphs from 6.0A will feature in this report as splitting could not be observed in lower current.

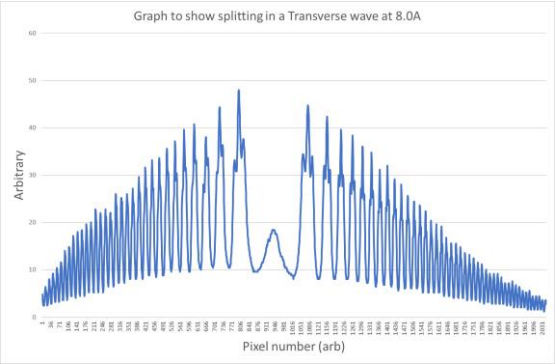

Figure 6 – A graph to show splitting in a Transverse wave at 8.0A

Figure 6 shows more succinctly the splitting in the energy levels as the magnetic field is stronger. Figures 5 and 6 are the results of the VideoCom Intensities plotted on a graph. These plots were then used to calculate the radii of the fringes produced by the constructive interference. To calculate these values the difference in the pixel number of the middle, inner and outer peaks was found.

These peaks and there splitting can be seen in the centre of graph, more prominently on figure 6. This gives the diameter of the pixel. These results were divided by two to find the radius of the pixel. This procedure was then repeated for all current readings from 6.0A to 8.0A for Transverse waves.

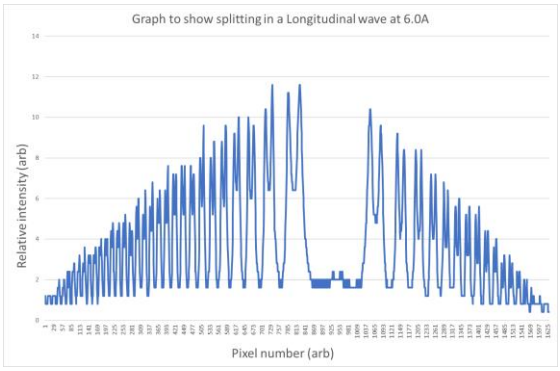

Figure 7 – A graph to show splitting in a Longitudinal wave at 6.0A.

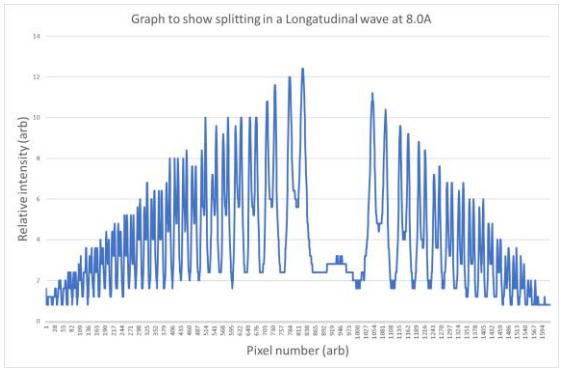

Figure 8 – A graph to show splitting in a Longitudinal wave at 8.0A.

Figures 7 and 8 both show the splitting in Longitudinal waves. The same process was done to calculate the radii on the pixel in Longitudinal waves as well as in Transverse waves. Once all these values had been recorded, they then had to be multiplied by $14\mu m$, as this is the width of 1 pixel. This was necessary to convert to the actual radii of the fringes. Looking at figures 7 and 8, the change in the plots is more subtle than the Transverse. Observing the peaks, you can notice the middle peaks have less relative intensity the stronger the magnetic field, also the inner and outer peaks lie slightly further apart to its corresponding peak.

Once a set of radii values had been collected the alpha values could be calculated.

$$\alpha = \frac{rk}{f}$$

Equation 12 – the equation to calculate alpha.

α (degrees)	α error (degrees)
0.0126	$\pm$9.609e-05
0.0130667	$\pm$9.882e-05
0.0131133	$\pm$9.908e-05
0.0130667	$\pm$9.882e-05
0.0130667	$\pm$9.882e-05
0.0130667	$\pm$9.882e-05
0.0130667	$\pm$9.882e-05
0.0130667	$\pm$9.882e-05
0.0130667	$\pm$9.882e-05
0.0131133	$\pm$9.909e-05
0.0130667	$\pm$9.882e-05

Table 1 – A table to show alpha values and their errors for the middle peak of the Transverse waves.

In table 1 you can see the results of one of the alpha value sets. To arrive at these values the radii of the fringes were divided by the focal length of the lenses (150mm) as shown in equation 12. Table 1 shows specifically the middle fringes for a Transverse wave however the process was done for every fringe for both waves.

$$\alpha_{err} = \sqrt{(\frac{rk_{err}}{rk})^2 + (\frac{f_{err}}{f})^2}\ \alpha$$

Equation 13 – Alpha error equation

Once all alpha values had been calculated, equation 13 was used to calculate the errors. The first error was the error on the pixel (rk_{err}), this error was taken to be half of 1 pixel ($\pm 7\mu m$) as 1 pixel was the resolution of VideoCom intensities. The other error was the focal length (f_{err}), the error given for this was $\pm 1mm$, this was the standard error quoted on the instrument. Both these errors were combined to give equation 13.

The next step of the analysis was to find values for $\frac{\Delta\lambda}{\lambda_0}$ using our alpha values. This was done by subbing in our alpha values into equation 10 where α_0 was the middle fringe and α_1 was either the outside or inside fringes. Once values were obtained for $\frac{\Delta\lambda}{\lambda_0}$ values were calculated for δE. This was done by multiplying together the results from equation 10 with equation 4.

δE (J)	δE error (J)
2.331e-24	$\pm$-4.089e-25
2.804e-24	$\pm$-4.383e-25
2.912e-24	$\pm$-4.417e-25
2.804e-24	$\pm$-4.388e-25
2.903e-24	$\pm$-4.390e-25
3.001e-24	$\pm$-4.397e-25
2.903e-24	$\pm$-4.390e-25
3.100e-24	$\pm$-4.403e-25
3.299e-24	$\pm$-4.417e-25
3.011e-24	$\pm$-4.423e-25
3.399e-24	$\pm$-4.424e-25

Table 2 – A table to show δE values and their errors for the outside fringes of a Transverse wave.

Table 2 shows the final values for δE and its errors. The errors were worked out by the following method:

$$\delta E_{err} = \sqrt{((\frac{\Delta\lambda}{\lambda_0}(\alpha_{1\,err}))^2_{err} + (\left(\frac{\Delta\lambda}{\lambda_0}(\alpha_{0\,err})\right)^2_{err}}\ (E_0)$$

Equation 14 - δE error equation

Equation 14 is the equation used to calculate the errors on δE, this equation was deduced by calculating the error on $\frac{\Delta\lambda}{\lambda_0}$ and multiplying it by α_{err}. The error calculations are too long to include in this section. For the full error calculation see appendix A.

The final error to include was the error on B. This was the simplest, as the standard error given by the Zeeman effect magnetic field calibration was 7mT.

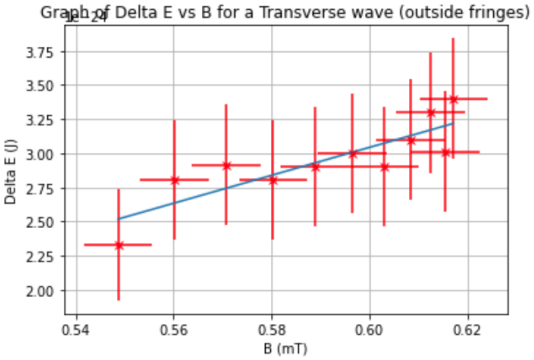

chi squared value = 0.12284696635051574

Figure 9 – A plot to show δE vs B for the outside fringes of a Transverse wave.

Figure 9 shows a positive gradient between δE and the magnetic field (B). As can be observed this graph's x and y axis are the same variables as in equation 3 (The energy during splitting). One of the aims of this experiment was to find a value for μ_B (the Bohr magneton), this means the gradient of the fit should produce a value for μ_B. The value obtained from figure 9 was $1.022e-23 \pm 2.056e-24\ J/T$, the actual value for μ_B is quoted as 9.274e-24 J/T [7] meaning the actual value lies within the error of our calculated value.

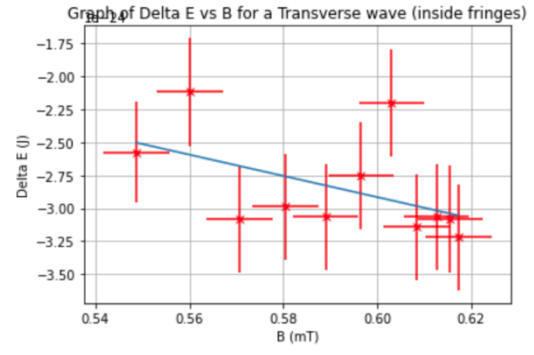

chi squared value = 0.7538982682249765

Figure 10 – A plot to show δE vs B for the inside fringes of a Transverse wave.

Figure 10 shows a negative gradient between δE and B, the calculated value for μ_B for this plot was $-8.053e-24 \pm 4.761e-24\ J/T$. For this graph, even though the error is bigger than the graph in figure 9 the value for μ_B is more accurate to the accepted. The chi squared values for both figures 9 and 10 are 0.122 and 0.754 respectively. These are excellent chi squired values as it shows the observed data is a good fit for the expected results.

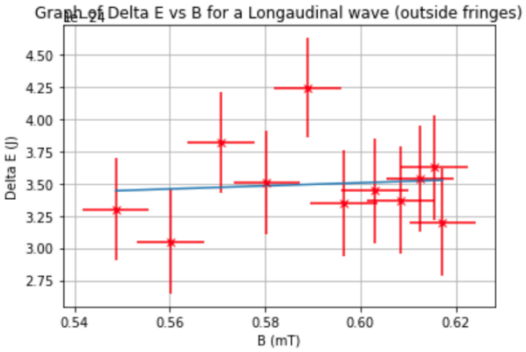

chi squared value = 0.7478623865285237

Figure 11 – A plot to show δE vs B for the outside fringes of a Longitudinal wave.

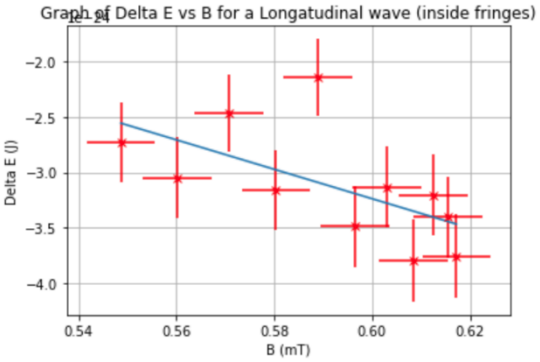

chi squared value = 1.4810467665916596

Figure 12 – A plot to show δE vs B for the inside fringes of a Longitudinal wave

In figures 11 and 12 the calculated values for μ_B were $1.198e-24 \pm 4.589e-24\ J/T$ and $1.331e-23 \pm 5.806e-24\ J/T$ respectively. It is clear to see from both these figures that the Longitudinal graphs are not as accurate as the Transverse. The line of best fit is supposed to show a positive gradient for figure 11 but does not as the data points are very spread out. This led to an inaccurate value for μ_B. Figure 12's plot is more accurate, however the chi squared value is over 1. This

means that the expected values are an overestimation of the observed values.

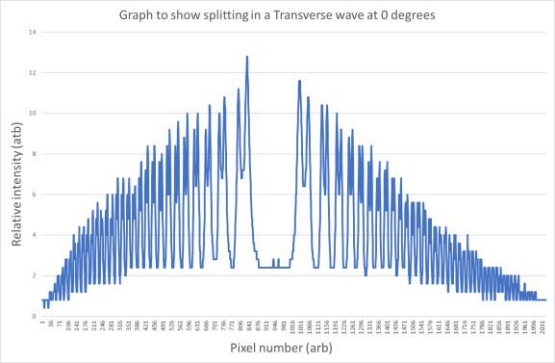

Figure 13 – A graph to show the polarisation of a Transverse wave at 0°.

If you look at the two centre peaks in figure 13 you can see they split down the middle, when compared to figure 5 (both 6.0A) you can see clearly the influence of the polarisation filter on the splitting.

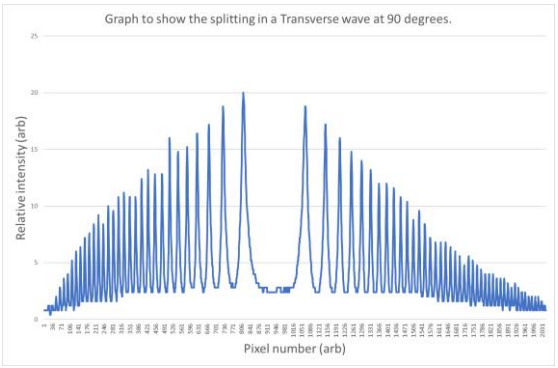

Figure 14 – A graph to show the polarization of a Transverse wave at 90°.

When comparing figure 14 to figure 13 you can see the clear distinction in polarisation. In both peaks on figure 14 you can see that there is no splitting observed. This shows that when the polarisation filter is set to 90° there is polarisation and when it's set to 0° none can be observed.

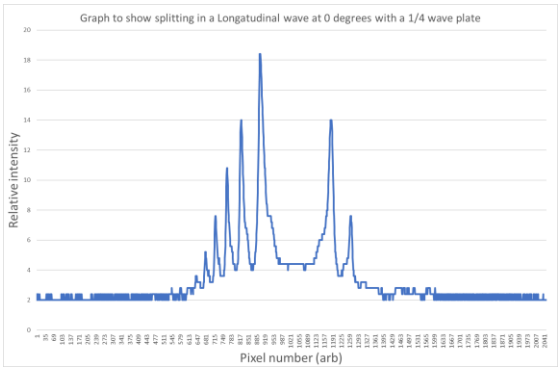

Figure 15 – A graph to show the polarisation of a Longitudinal wave at 0° *with a ¼ wave plate*

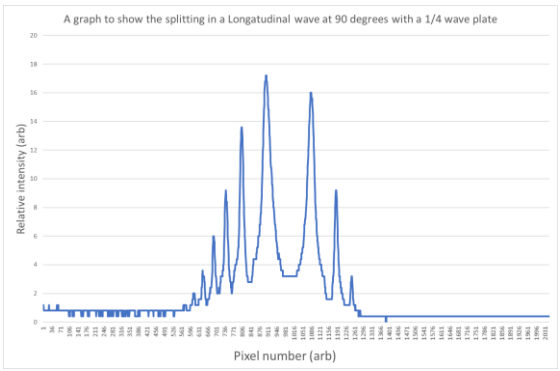

Figure 16 - – A graph to show the polarisation of a Longitudinal wave at 90° *with a ¼ wave plate*

Figures 15 and 16 show the polarization of Longitudinal waves at $0^{\circ}$and $90^{\circ}$for a ¼ wave plate respectively. For these plots to be produced the standard polarization filter was kept constant at 0° while the ¼ wave plate was varied. Looking at both figures you can see that distance in pixel number between the peaks shortens as the angle increases as the circular polarized plate changes to plain polarized light.

5. Discussion

Three out of four values for the Bohr magneton lie within the error of the accepted value. This shows that despite some discrepancies the experiment was successful in completing its main aim. Figure 11 was the only plot to not have the obtained value error fall within the actual. This is because the data points on figure 11 are quite spread out. When the radii fringes were recorded it was found that that they only increased very slightly as the magnetic field became stronger

and in some cases the radii stayed the same. This could be because as the current increased the Longitudinal plots did not vary by a great amount, causing similar splitting graphs at different currents. This can be seen in figures 7 and 8. Overall this caused the Longitudinal graphs to be less accurate.

The error bars on figures 9 to 12 were relatively large, especially on δE as they were 10% of the calculated values. The main experimental errors that led to these results were the error on the radii (error on the pixel) and the error on the focal lens. The error on the radii will come from the pixel error from VideoCom intensities. This error could have been reduced if the software had a higher resolution so as a result a more accurate plot could be taken. There could also be some discrepancy in working out the difference in the peaks. It is difficult to work out by eye the exact tip of the peaks. This would lead to inaccurate radii values and would explain the poor data in figure 11.

The error in the focal lenses could be improved by using more accurate lenses with a lower error on the instrument. This would lead to more accurate values of α.

The polarization graphs in figures 13 and 14 do accurately show the transition from splitting to no splitting while keeping the current constant. However, the Longitudinal graphs in figures 15 and 16 while they do vary, it is difficult to notice a large dissimilarity in them, making it difficult to determine the polarisation states. The errors in the polarisation would be the same as previously mentioned.

Overall, if this experiment was to be repeated it could be improved by using more precise equipment as to reduce the standard errors. More readings could also be taken. In this experiment time was limited and the current was limited as it was unsafe to go above 8.0A. With more time, readings could be taken every 0.1A to produce more data points and with a higher current the physical characteristics of splitting would be easier to observe.

6. Conclusion

To conclude, The Zeeman effect is the splitting of energy levels in a magnetic field. This experiment is performed by applying current to create a magnetic field around a Cadmium lamp. The light given off from this lamp is then observed by a CCD camera where the splitting can be seen in high currents of 6.0A or above. The process was done for both Transverse and Longitudinal waves, after this polarisation filters were added to the equipment to be able to determine the polarisation states.

The results obtained from this experiment were accurate to the accepted values, all but one falling within the error for the Bohr magneton. The change in the angle used to determine the polarisation states also effectively showed how the splitting changed with the angle. If this experiment was to be performed again more accurate equipment and software would be needed to gain better results.

7. References

[1] - Linda Hall Library. 2021. *Pieter Zeeman - Scientist of the Day - Linda Hall Library*. [online] Available at: <https://www.lindahall.org/pieter-zeeman/> [Accessed 22 October 2021].

[2] - Hyperphysics.phy-astr.gsu.edu. 2021. *Zeeman Effect*. [online] Available at: <http://hyperphysics.phy-astr.gsu.edu/hbase/quantum/zeeman.html> [Accessed 22 October 2021].

[3] - Encyclopaedia Britannica. 2021. *Zeeman effect | physics*. [online] Available at: <https://www.britannica.com/science/Zeeman-effect> [Accessed 22 October 2021].

[4] - www.dictionary.com. 2021. *Definition of quantize | Dictionary.com*. [online] Available at:

<https://www.dictionary.com/browse/quantized> [Accessed 22 October 2021].

[5] - Getkisi.com. 2021. *CCD Camera: What Is It and How Does It Work | Kisi*. [online] Available at: <https://www.getkisi.com/guides/ccd-camera> [Accessed 23 October 2021].

[6] - 2021. [online] Available at: <https://www.knightoptical.com/news/the-value-of-condenser-lenses-in-projection-systems/> [Accessed 23 October 2021].

[7] - Physics.nist.gov. 2021. *CODATA Value: Bohr magneton*. [online] Available at: <https://physics.nist.gov/cgi-bin/cuu/Value?mub> [Accessed 23 October 2021].

8. Appendix A – error calculation

Error calculation for equation 14:

Start by differentiating the numerator in equation 10:

$$(\frac{\Delta\lambda}{\lambda_0})_{in\ or\ out\ err} = -\frac{\left(\frac{\cos(\alpha_1)\sin(\alpha_1)}{n^2\sqrt{1-\frac{\sin(\alpha_1)^2}{n^2}}}\right)}{\sqrt{1-\frac{\sin(\alpha_0)^2}{n^2}}}$$

Then differentiate the denominator:

$$(\frac{\Delta\lambda}{\lambda_0})_{mid\ err} = \frac{\cos(\alpha_0)\sin(\alpha_0)}{n^2(1-\left(\frac{\sin(\alpha_0)^2}{n^2}\right)^{\frac{3}{2}}}(\sqrt{1-\frac{\sin(\alpha_1)^2}{n^2}})$$

Times by the error on alpha:

$$\left(\frac{\Delta\lambda}{\lambda_0}\right)_{in\ or\ out\ err}(\alpha_{1\ err})$$

$$\left(\frac{\Delta\lambda}{\lambda_0}\right)_{mid\ err}(\alpha_{0\ err})$$

Combine both equations:

$$\delta E_{err} = \sqrt{((\frac{\Delta\lambda}{\lambda_0}(\alpha_1))^2_{out/in\ err} + ((\frac{\Delta\lambda}{\lambda_0}(\alpha_0))^2_{mid\ err}}$$

Then multiply by E_0:

$$\delta E_{err} = \sqrt{((\frac{\Delta\lambda}{\lambda_0}(\alpha_{1\ err}))^2_{\frac{out}{in}err} + (\left(\frac{\Delta\lambda}{\lambda_0}(\alpha_{0\ err})\right)^2_{mid\ err}}(E_0)$$

This is the final equation.

9. Appendix B – Other relevant information

Derivation for equation 8 from 7:

Look at figure 2 for trigonometry section.

$$OPD = k\lambda = 2nA - B$$

Using trigonometry:

$$A = \frac{d}{\cos(\beta)}$$

$$x = dTan(\beta)$$

Triangle 2:

$$B = 2\text{x}\sin(\alpha)$$

$$B = 2dsin(\alpha)Tan(\beta)$$

Kλ:

$$k\lambda = \frac{2nd}{\cos(\beta)} - 2dsin(\alpha)Tan(\beta)$$

$$n_0\sin(\alpha) = nsin(\beta)$$

As $n_0 = 1$:

$$\sin(\alpha) = nsin(\beta)$$

$$\frac{2nd}{\cos(\beta)} = \frac{2nd\sin(\beta)^2}{\cos(\beta)}$$

$$\frac{2nd}{\cos(\beta)}(1 - \sin(\beta)^2)$$

$$\frac{2nd}{\cos(\beta)}(\cos(\beta)^2)$$

$$2ndcos(\beta)$$

$$2nd\sqrt{1-\sin(\beta)^2}$$

$$2nd(\sqrt{1-\frac{\sin(\alpha)^2}{n^2}})$$

$$2nd(\sqrt{\frac{n^2-\sin(\alpha)^2}{n^2}})$$

$$2nd(\sqrt{\frac{n^2-\sin(\alpha)^2}{n}})$$

$$OPD = k\lambda = 2d\sqrt{n^2-\sin(\alpha)^2}$$

This is the final equation.

Derivation for equation 10 from 8:

$$k\lambda = 2d\sqrt{n^2-\sin(\alpha)^2}$$

$$\lambda_0 = \frac{2d}{k}\sqrt{n^2-\sin(\alpha_0)^2}$$

$$\lambda_1 = \frac{2d}{k}\sqrt{n^2-\sin(\alpha_1)^2}$$

Combine λ_0 and λ_1:

$$\frac{\Delta\lambda}{\lambda_0} = \frac{\lambda_1-\lambda_0}{\lambda_0}$$

$$= \frac{\frac{2d}{k}(\sqrt{n^2-\sin(\alpha_1)^2}-\sqrt{n^2-\sin(\alpha_0)^2})}{\frac{2d}{k}\sqrt{n^2-\sin(\alpha_0)^2}}$$

$$\frac{\Delta\lambda}{\lambda_0} = \frac{(\sqrt{n^2-\sin(\alpha_1)^2}-\sqrt{n^2-\sin(\alpha_0)^2})}{\sqrt{n^2-\sin(\alpha_0)^2}}$$

$$\frac{\Delta\lambda}{\lambda_0} = \frac{\sqrt{n^2-\sin(\alpha_1)^2}}{\sqrt{n^2-\sin(\alpha_0)^2}} - 1$$

This is the final equation.